

# NuFIT: Three-Flavour Global Analyses of Neutrino Oscillation Experiments

M.C. Gonzalez-Garcia<sup>1,2,3</sup> , Michele Maltoni<sup>4</sup> , Thomas Schwetz<sup>5</sup> 

<sup>1</sup> Institució Catalana de Recerca i Estudis Avançats (ICREA),

<sup>2</sup> Departament d'Estructura i Constituents de la Matèria, Universitat de Barcelona, 647 Diagonal, E-08028 Barcelona, Spain

<sup>3</sup> C.N. Yang Institute for Theoretical Physics, SUNY at Stony Brook, Stony Brook, NY 11794-3840, USA

<sup>4</sup> Instituto de Física Teórica UAM/CSIC, Calle de Nicolás Cabrera 13–15, Universidad Autónoma de Madrid, Cantoblanco, E-28049 Madrid, Spain

<sup>5</sup> Institut für Astroteilchenphysik, Karlsruher Institut für Technologie (KIT), D-76021 Karlsruhe, Germany

\* E-mails: concha@insti.physics.sunysb.edu, michele.maltoni@csic.es, schwetz@kit.edu

**Abstract:** In this contribution we summarize the determination of neutrino masses and mixing arising from the global analysis of data from atmospheric, solar, reactor, and accelerator neutrino experiments performed in the framework of three-neutrino mixing and obtained in the context of the NuFIT collaboration. Apart from presenting the latest status as of fall 2021, we discuss the evolution of the global fit results over the last ten years, and mention various pending issues (and their resolution) which occurred during that period in the global analyses.

**Keywords:** Neutrino oscillation, neutrino physics, NuFIT

## 1. Introduction

The observation of flavour transitions in neutrino propagation in a variety of experiments has established beyond doubt that lepton flavours are not symmetries of Nature. And the dependence of the probability of the observed flavour transitions with the distance traveled by the neutrinos and their energy has allowed to single out neutrino masses and the mixing in the weak charged current interactions of the massive neutrino states as the responsible mechanism for the observed flavour oscillations [1,2]. (see Ref. [3] for an overview).

At the time of the writing of this mini-review neutrino oscillation effects have been observed in:

- $\nu_e$ ,  $\nu_\mu$ ,  $\bar{\nu}_e$ , and  $\bar{\nu}_\mu$ , atmospheric neutrinos, produced by the interaction of the cosmic rays on the top of the atmosphere. At present the results with highest statistics correspond to the Super-Kamiokande [4] and IceCube/DeepCore [5,6] experiments;
- $\nu_e$  solar neutrinos, produced in the nuclear reactions which make the Sun shine. Results included in the present determination of the flavour evolution of solar neutrinos comprise the total event rates in radiochemical experiments Chlorine [7], Gallex/GNO [8], and SAGE [9], and the time and energy dependent rates in the four phases of Super-Kamiokande [10–13], the three phases of SNO [14], and Borexino [15–17];
- neutrinos produced in accelerators and detected at distance  $\mathcal{O}(100 \text{ km})$ , in the so-called long baseline (LBL) experiments, and in which neutrino oscillations have been observed in two channels
  - disappearance results in the energy distribution of  $\nu_\mu$  and  $\bar{\nu}_\mu$  events which have been precisely measured in MINOS [18], T2K [19] and NOvA [20];
  - appearance results of both  $\nu_e$  and  $\bar{\nu}_e$  events also in their energy distribution detected in MINOS [21], T2K [19] and NOvA [20];



**Citation:** Gonzalez-Garcia, M.C.; Maltoni, M.; Schwetz, T. NuFIT: Three-Flavour Global Analyses of Neutrino Oscillation Experiments. *Preprints* **2021**, *1*, 0. <https://doi.org/>

Received:

Accepted:

Published:

**Publisher's Note:** MDPI stays neutral with regard to jurisdictional claims in published maps and institutional affiliations.

- $\bar{\nu}_e$  produced in nuclear reactors. Their disappearance has been observed in their measured energy spectrum at two distinctive baselines
  - at  $\mathcal{O}(1 \text{ km})$ , here denoted medium baselines (MBL), in Double Chooz [22], Daya Bay [23], and RENO [24];
  - at LBL in KamLAND [25].

As we will argue below these results imply that *neutrinos are massive and there is physics beyond the Standard Model (BSM)*.

The first step towards the discovery of the underlying BSM dynamics for neutrino masses is the detailed characterization of the minimal low energy parametrization able of describing the bulk of results. This requires global analysis of the oscillation data as they become available. At present, such combined analysis are in the hands of a few phenomenological groups (see for example [26–29]). The NuFIT Collaboration [30] was formed in this context about one decade ago by the three authors of this article, with the goal of providing timely updated global analysis of neutrino oscillation measurements determining the leptonic mixing matrix and the neutrino masses in the framework of the Standard Model extended with three massive neutrinos. We have published five major updates of the analysis [31–36], while intermediate updates have been regularly posted in the NuFIT website [30]. Over the years the work of a number of graduate students and postdocs has been paramount to the success of the project: Johannes Bergström [33], Ivan Esteban [34–36], Alvaro Hernandez-Cabezudo [35], Ivan Martinez-Soler [34], Jordi Salvado [31], and Albert Zhou [36].

## 2. The New Minimal Standard Model with Three Massive Neutrinos

The Standard Model (SM) is a gauge theory built to explain the strong, weak and electromagnetic interactions of all known elementary particles. It is based on the gauge symmetry  $SU(3)_{\text{Color}} \times SU(2)_{\text{Left}} \times U(1)_Y$  and it is spontaneously broken to  $SU(3)_{\text{Color}} \times U(1)_{\text{EM}}$  by the Higgs mechanism which provides a vacuum expectation value for a Higgs  $SU(2)_{\text{Left}}$  doublet field  $\phi$ . The SM contains three fermion generations and the chiral nature of the  $SU(2)_{\text{Left}}$  part of the gauge group — partly responsible for the weak interactions — implies that right-handed and left-handed fermions experiment different weak interactions. Left-handed fermions are assigned to the  $SU(2)_{\text{Left}}$  doublet representation while right-handed fermions are  $SU(2)_{\text{Left}}$  singlets. Conversely because of the vector nature of  $SU(3)_{\text{Color}}$  and  $U(1)_{\text{EM}}$  interactions, both left-handed and right-handed fermion fields are required to build the electromagnetic and strong currents. Neutrinos are the only fermions which do not have neither color nor electric charge. They only feel weak interactions. Consequently the right-handed neutrinos are singlets of the full SM group and therefore have no place in the SM of particle interactions.

As a consequence of the gauge symmetry and the group representations in which the fermions are assigned, the SM possesses the accidental global symmetry  $U(1)_B \times U(1)_e \times U(1)_\mu \times U(1)_\tau$  where  $U(1)_B$  is the baryon number symmetry, and  $U(1)_{e,\mu,\tau}$  are the three lepton flavour symmetries.

In the SM fermion masses are generated by the Yukawa interactions which couple the right-handed fermion ( $SU(2)_{\text{Left}}$ -singlet) to the left-handed fermion ( $SU(2)_{\text{Left}}$ -doublet) and the Higgs doublet. After electroweak spontaneous symmetry breaking these interactions provide charged fermion masses. On the contrary, no Yukawa interaction can be written that would give mass to the neutrino because no right-handed neutrino exists in the model. Furthermore, any neutrino mass term built with the left-handed neutrino fields would violate  $U(1)_{L=L_e+L_\mu+L_\tau}$ , which is a subgroup of the accidental symmetry group. As such it cannot be generated by loop corrections within the model. Also, it cannot be generated by non-perturbative corrections because the  $U(1)_{B-L}$  subgroup of the global symmetry is non-anomalous.

From these arguments it follows that the SM predicts that neutrinos are *strictly* massless. It also implies that there is no leptonic flavour mixing and that there is not possibility of CP violation of the leptons. But, as described in the introduction, we have now undoubted experimental evidence that leptonic flavours are not conserved in neutrino propagation. Consequently the Standard Model has to be extended.

The simplest extension capable of describing the experimental observations must include neutrino masses. Let us call this minimal extension the *New Minimal Standard Model* (NMSM). In fact, such simplest extension is not unique because, unlike for charged fermions, one can construct a neutrino mass term in two different forms:

- in one minimal extension one introduces the right-handed neutrinos,  $\nu_R$ , and imposes that total lepton number is still conserved. In this form gauge invariance allows for a Yukawa interaction involving  $\nu_R$  and the lepton doublet — in analogy to the charged fermions — so, after electroweak spontaneous symmetry breaking the NMSM Lagrangian reads:

$$\mathcal{L}_D = \mathcal{L}_{\text{SM}} - M_\nu \bar{\nu}_L \nu_R + \text{h.c.} \quad (1)$$

In this case the neutrino mass eigenstates are Dirac fermions, and neutrino and anti neutrinos are distinct fields *i.e.*,  $\nu^c \neq \nu$  (here  $\nu^c$  represents the charge conjugate neutrino field). This NMSM is gauge invariant under the SM gauge group;

- in another minimal extension one constructs a mass term employing only the SM left-handed neutrinos by allowing the violation of total lepton number. In this case the NMSM Lagrangian is:

$$\mathcal{L}_M = \mathcal{L}_{\text{SM}} - \frac{1}{2} M_\nu \bar{\nu}_L \nu_L^c + \text{h.c.} \quad (2)$$

In this NMSM the mass eigenstates are Majorana fermions,  $\nu^c = \nu$ . The Majorana mass term above breaks the electroweak gauge invariance.

Consequently  $\mathcal{L}_M$  can only be understood as a low energy limit of a complete theory while  $\mathcal{L}_D$  is formally self-consistent. But in either NMSM lepton flavours are mixed in the charged-current interactions of the leptons. This is, if we denote the neutrino mass eigenstates by  $\nu_i$ , with  $i = 1, 2, \dots$ , and the charged lepton mass eigenstates by  $l_i = (e, \mu, \tau)$ , then leptonic charged-current interactions of those massive states are given by

$$- \mathcal{L}_{\text{CC}} = \frac{g}{\sqrt{2}} \bar{l}_{iL} \gamma^\mu U^{ij} \nu_j W_\mu^+ + \text{h.c.} \quad (3)$$

where  $U$  is the leptonic mixing matrix analogous to the CKM matrix for the quarks. Leptonic mixing generated this way is, however, slightly more general than the CKM flavour mixing of quarks because the number of massive neutrinos (lets call it  $n$ ) is unknown. This is so because right-handed neutrinos are SM-singlets and therefore there are no constraints on their number. And also, as mentioned above, unlike charged fermions, neutrinos can be Majorana particles. As a consequence the number of new parameters in the model NMSM depends on the number of massive neutrino states and on whether they are Dirac or Majorana particles.

In most generality  $U$  in Eq. (3) is a  $3 \times n$  matrix, and verifies  $UU^\dagger = I_{3 \times 3}$  but in general  $U^\dagger U \neq I_{n \times n}$ . In this review, however, we will be focusing on analyses made in the context of only three neutrino massive states, which is the simplest scheme to consistently describe the data listed in the introduction. In this case the three known neutrinos ( $\nu_e, \nu_\mu, \nu_\tau$ ) can be

**Table 1.** Experiments contributing to the present determination of the oscillation parameters.

Experiment	Dominant	Important
Solar Experiments	$\theta_{12}$	$\Delta m_{21}^2, \theta_{13}$
Reactor LBL (KamLAND)	$\Delta m_{21}^2$	$\theta_{12}, \theta_{13}$
Reactor MBL (Daya Bay, RENO, Double Chooz)	$\theta_{13},  \Delta m_{3\ell}^2 $	—
Atmospheric Experiments (SK, IC-DC)	—	$\theta_{23},  \Delta m_{3\ell}^2 , \theta_{13}, \delta_{\text{CP}}$
Accel LBL ( $\nu_\mu, \bar{\nu}_\mu$ ) disapp (K2K, MINOS, T2K, NOvA)	$ \Delta m_{3\ell}^2 , \theta_{23}$	—
Accel LBL ( $\nu_e, \bar{\nu}_e$ ) appearance (MINOS, T2K, NOvA)	$\delta_{\text{CP}}$	$\theta_{13}, \theta_{23}$

expressed as quantum superpositions of three massive states  $\nu_i$  ( $i = 1, 2, 3$ ) with masses  $m_i$ , and the leptonic mixing matrix can be parametrized as [37]:

$$U = \begin{pmatrix} 1 & 0 & 0 \\ 0 & c_{23} & s_{23} \\ 0 & -s_{23} & c_{23} \end{pmatrix} \begin{pmatrix} c_{13} & 0 & s_{13}e^{-i\delta_{\text{CP}}} \\ 0 & 1 & 0 \\ -s_{13}e^{i\delta_{\text{CP}}} & 0 & c_{13} \end{pmatrix} \begin{pmatrix} c_{21} & s_{12} & 0 \\ -s_{12} & c_{12} & 0 \\ 0 & 0 & 1 \end{pmatrix} \begin{pmatrix} e^{i\alpha_1} & 0 & 0 \\ 0 & e^{i\alpha_2} & 0 \\ 0 & 0 & 1 \end{pmatrix}, \quad (4)$$

where  $c_{ij} \equiv \cos \theta_{ij}$  and  $s_{ij} \equiv \sin \theta_{ij}$ . In addition to the Dirac-type phase  $\delta_{\text{CP}}$ , analogous to that of the quark sector, there are two physical phases  $\alpha_1, \alpha_2$  associated to a possible Majorana character of neutrinos, which, however, are not relevant for neutrino oscillations.

A consequence of the presence of neutrino masses and the leptonic mixing is the possibility of mass-induced flavour oscillations in vacuum [1,2], as well as the possibility of flavour transitions when neutrino traverses regions of dense matter [38,39]. Generically the flavour transition probability in vacuum presents an oscillatory  $L$  dependence with phases proportional to  $\sim \Delta m^2 L / E$  and amplitudes proportional to different elements of mixing matrix. The presence of matter in the neutrino propagation alters both the oscillation frequencies and the amplitudes (see Ref. [3] for an overview).

In the convention of Eq. (4), disappearance of solar  $\nu_e$ 's and long baseline reactor  $\bar{\nu}_e$ 's dominantly proceed via oscillations with wavelength  $\propto E / \Delta m_{21}^2$  ( $\Delta m_{ij}^2 \equiv m_i^2 - m_j^2$  and  $\Delta m_{21}^2 \geq 0$  by convention) and amplitudes controlled by  $\theta_{12}$ , while disappearance of atmospheric and LBL accelerator  $\nu_\mu$ 's dominantly proceed via oscillations with wavelength  $\propto E / |\Delta m_{31}^2| \ll E / \Delta m_{21}^2$  and amplitudes controlled by  $\theta_{23}$ . Generically  $\theta_{13}$  controls the amplitude of oscillations involving  $\nu_e$  flavour with  $E / |\Delta m_{31}^2|$  wavelengths. The angles  $\theta_{ij}$  can be taken to lie in the first quadrant,  $\theta_{ij} \in [0, \pi/2]$ , and the phase  $\delta_{\text{CP}} \in [0, 2\pi]$ . Values of  $\delta_{\text{CP}}$  different from 0 and  $\pi$  imply CP violation in neutrino oscillations in vacuum. In this convention  $\Delta m_{21}^2$  is positive by construction. Moreover given the observed hierarchy between the solar and atmospheric wavelengths there are two possible non-equivalent orderings for the mass eigenvalues

- $m_1 \ll m_2 < m_3$  so  $\Delta m_{21}^2 \ll \Delta m_{32}^2 (\simeq \Delta m_{31}^2 > 0)$ , refer to as Normal ordering (NO);
- $m_3 \ll m_1 < m_2$  so  $\Delta m_{21}^2 \ll -(\Delta m_{31}^2 \simeq \Delta m_{32}^2 < 0)$  refer to as Inverted ordering (IO)

The two ordering, therefore, correspond to the two possible choices of the sign of  $\Delta m_{31}^2$ . In NUFIT we adopted the convention of reporting results for  $\Delta m_{31}^2$  for NO and  $\Delta m_{32}^2$  for IO, *i.e.*, we always use the one which has the larger absolute value. Sometimes we will generically denote such quantity as  $\Delta m_{3\ell}^2$ , with  $\ell = 1$  for NO and  $\ell = 2$  for IO.

In summary, the  $3\nu$  oscillation analysis of the existing data involves a total of six parameters: two mass-squared differences (one of which can be positive or negative), three mixing angles, and the CP phase  $\delta_{\text{CP}}$ . For the sake of clarity we summarize in Table 1 which experiment contribute dominantly to the present determination of the different parameters.

### 3. NuFIT Results: The Three-Neutrino Paradigm

The latest determination of the six parameters in the new NMSM are presented in Table 2. They correspond to the NuFIT 5.1 analysis [30,36]. The progress in the determination of these parameters over the last decade is illustrated in Fig. 1 where we show the one-dimensional projections of the  $\Delta\chi^2$  from the global analysis as a function of each of the six parameters, obtained in the first NuFIT 1.0 analysis and the last NuFIT 5.1 in the upper and lower row respectively.

To further illustrate the improvement on the robust precision on the determination of these parameters over the last decade we can compute the  $3\sigma$  relative precision of parameter  $x$

$$\frac{2(x^+ - x^-)}{(x^+ + x^-)}$$

where  $x^+$  and  $x^-$  are the upper and lower bounds on parameter  $x$  at the  $3\sigma$  level. Doing so we find the following change in the  $3\sigma$  relative precision (marginalizing over ordering):

	NuFIT 1.0	NuFIT 2.0	NuFIT 3.0	NuFIT 4.0	NuFIT 5.1
$\theta_{12}$	15%	14%	14%	14%	14%
$\theta_{13}$	30%	15%	11%	8.9%	9.0%
$\theta_{23}$	43%	32%	32%	27%	27%
$\Delta m_{21}^2$	14%	14%	14%	16%	16%
$ \Delta m_{3\ell}^2 $	17%	11%	9%	7.8%	6.7% [6.5%]
$\delta_{\text{CP}}$	100%	100%	100%	100% [92%]	100% [83%]
$\Delta\chi_{\text{IO-NO}}^2$	$\pm 0.5$	$-0.97$	$+0.83$	$+4.7$ [+9.3]	$+2.6$ [+7.0]

(5)

where in the last two columns the numbers between brackets show the impact of including the tabulated SK-atm data (see Sec. 3.3) in the precision of the determination of such parameter. Since the  $\Delta\chi^2$  profile of  $\delta_{\text{CP}}$  is not Gaussian the precision estimation above for  $\delta_{\text{CP}}$  is only indicative. In addition we show in the last line the  $\Delta\chi^2$  between orderings which for NuFIT 1.0 changed from  $+0.5$  to  $-0.5$  depending on the choice of normalization for the reactor fluxes.

Besides the expected improvement on the precision associated with the increased statistics of some of the experiments and the addition of data from new experiments, there were a number of issues entering the analysis which changed over the period covered. Next we briefly comment on those.

#### 3.1. Reactor Neutrino Flux Uncertainties

The NuFIT 1.0 analysis came out soon after the first results from the medium baseline ( $\mathcal{O}(1 \text{ km})$ ) reactor experiments Daya Bay [40], RENO [41], and Double Chooz [42] provided a positive determination of the mixing angle  $\theta_{13}$ . The data from those experiments was analyzed together with that from the finalized reactor experiments Chooz [43] and Palo Verde [44]. The analysis of reactor experiments without a near detector, in particular Chooz, Palo Verde and the early measurements of Double Chooz, depends on the expected rates as computed with some prediction for the neutrino fluxes from the reactors.

At about the same time, the so called *reactor anomaly* was first pointed out. It amounted to the fact that the most updated reactor flux calculations in Refs. [45–47] resulted in an increase of the predicted fluxes and a reduction of the uncertainties. Compared to those fluxes, the results from finalized reactor experiments at baselines  $\lesssim 100 \text{ m}$  such as Bugey4 [48], ROVNO4 [49], Bugey3 [50], Krasnoyarsk [51,52], ILL [53], Gösgen [54], SRP [55], and ROVNO88 [56] had observed a deficit. In the framework of three flavour oscillations these reactor short-baseline experiments (RSBL) are not sensitive to oscillations but at the time played an important role

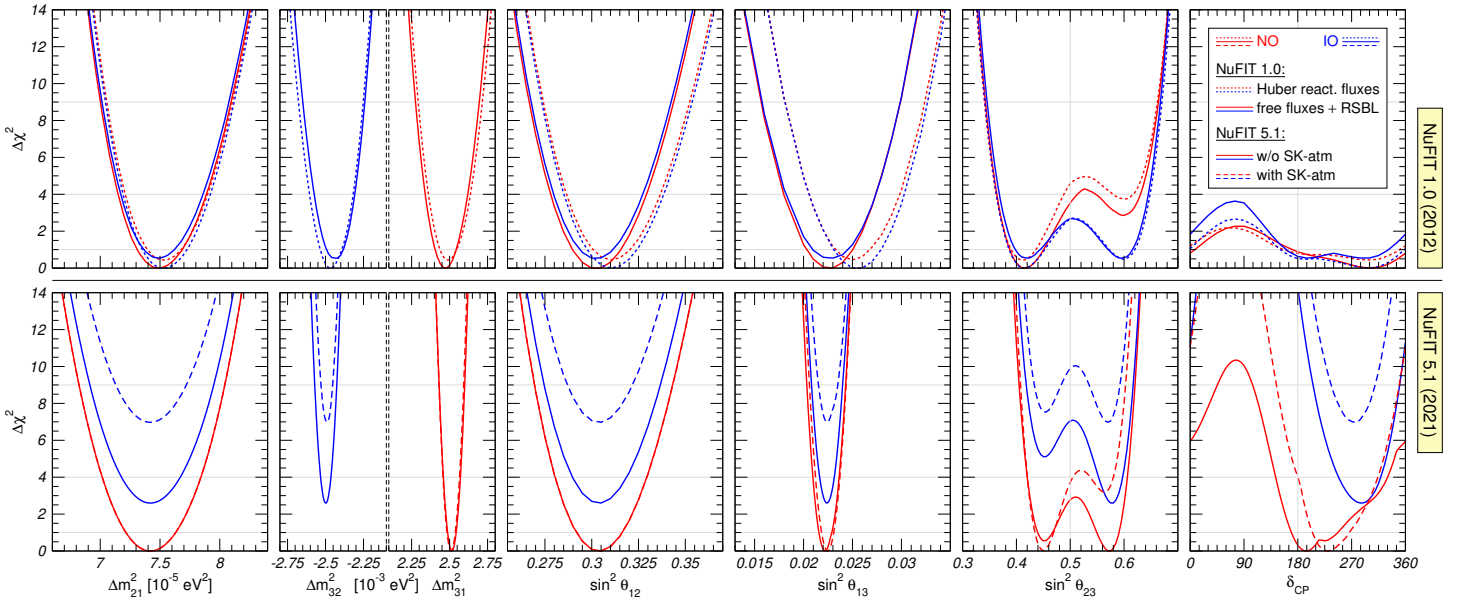


**Figure 1.** Comparison of the global  $3\nu$  oscillation analysis results. In all panels we show  $\Delta\chi^2$  profiles minimized with respect to all undisplayed parameters. The red (blue) curves are for Normal (Inverted) Ordering. Note that as atmospheric mass-squared splitting we use  $\Delta m_{31}^2$  for NO and  $\Delta m_{32}^2$  for IO. **Top:** NuFIT 1.0 results (adapted from Ref. [31]). Solid curves were obtained with free normalization of reactor fluxes and the inclusion of data from short-baseline (less than 100 m) reactor experiments, while for the dotted curves short-baseline data are *not* included but reactor fluxes are fixed to the predictions of Ref. [46]. **Bottom:** NuFIT 5.1 results. In all curves the neutrino fluxes for each reactor experiment are constrained by the corresponding near detector. Solid (dashed) curves are obtained without (with) the inclusion of the tabulated SK-atm  $\Delta\chi^2$  data.

in constraining the unoscillated reactor neutrino flux. So they could be used as an alternative to the theoretically calculated reactor fluxes.

The dependence of these early determinations of  $\theta_{13}$  on the reactor flux modeling is illustrated in Fig. 2. The upper panels contain the  $\Delta\chi^2$  from Chooz, Palo Verde, Double Chooz, Daya Bay and RENO as a function of  $\theta_{13}$  for different choices for the reactor fluxes. From the upper-left panel we read that when the fluxes from Ref. [46] were employed and the RSBL reactor experiments were not included in the fit, all experiments, including Chooz and Palo Verde, preferred  $\theta_{13} > 0$ . However when the RSBL reactor experiments were added to the fit such preference vanished [57], and that happened independently of whether the flux normalization  $f_{\text{flux}}$  was left as a free parameter or not. This can also be inferred from the lower-left panel which shows the contours in the  $(\theta_{13}, f_{\text{flux}})$  plane for the analysis of Chooz and Palo Verde with and without the inclusion of RSBL data. The central panels show the dependence of the determination of  $\theta_{13}$  from the analysis of Double Chooz on the choice of reactor fluxes: as can be seen, the best fit value as well as the statistical significance of the non-zero  $\theta_{13}$  signal in this experiment depended significantly on the reactor flux assumption. This was due to the lack of the near detector in Double Chooz at the time.

In view of this, and in order to properly assess the impact of the reactor anomaly on the allowed range of neutrino parameters in NuFIT 1.0, the global analysis was performed under two extreme choices. In the first choice (labeled “Free fluxes + RSBL” in Fig. 1) we left the normalization of reactor fluxes free and included the data from RSBL experiments. In the second option (labeled “Huber”) we did not include the RSBL data and assume reactor fluxes and uncertainties as predicted in Ref. [46]. As can be seen in the left panels of Fig. 1, this choice resulted in an additional uncertainty of about  $1\sigma$  on various observables.



**Table 2.** Present determination of the three-flavour oscillation parameters from the fit to global data NuFIT 5.1 [30,36]. The results in the first and second column correspond to the analysis performed under the assumption of NO and IO respectively, and therefore they are confidence intervals defined relative to the respective local minimum. The results shown in the upper and lower sections correspond to analysis performed without and with the addition of the tabulated SK-atm  $\Delta\chi^2$  data respectively. In quoting the values for the largest mass splitting we have defined  $\Delta m_{3\ell}^2 \equiv \Delta m_{31}^2 > 0$  for NO and  $\Delta m_{3\ell}^2 \equiv \Delta m_{32}^2 < 0$  for IO.

		Normal Ordering (best fit)		Inverted Ordering ( $\Delta\chi^2 = 2.6$ )	
		bfp $\pm 1\sigma$	$3\sigma$ range	bfp $\pm 1\sigma$	$3\sigma$ range
without SK atmospheric data	$\sin^2 \theta_{12}$	$0.304^{+0.013}_{-0.012}$	$0.269 \rightarrow 0.343$	$0.304^{+0.012}_{-0.012}$	$0.269 \rightarrow 0.343$
	$\theta_{12}/^\circ$	$33.44^{+0.77}_{-0.74}$	$31.27 \rightarrow 35.86$	$33.45^{+0.77}_{-0.74}$	$31.27 \rightarrow 35.87$
	$\sin^2 \theta_{23}$	$0.573^{+0.018}_{-0.023}$	$0.405 \rightarrow 0.620$	$0.578^{+0.017}_{-0.021}$	$0.410 \rightarrow 0.623$
	$\theta_{23}/^\circ$	$49.2^{+1.0}_{-1.3}$	$39.5 \rightarrow 52.0$	$49.5^{+1.0}_{-1.2}$	$39.8 \rightarrow 52.1$
	$\sin^2 \theta_{13}$	$0.02220^{+0.00068}_{-0.00062}$	$0.02034 \rightarrow 0.02430$	$0.02238^{+0.00064}_{-0.00062}$	$0.02053 \rightarrow 0.02434$
	$\theta_{13}/^\circ$	$8.57^{+0.13}_{-0.12}$	$8.20 \rightarrow 8.97$	$8.60^{+0.12}_{-0.12}$	$8.24 \rightarrow 8.98$
	$\delta_{\text{CP}}/^\circ$	$194^{+52}_{-25}$	$105 \rightarrow 405$	$287^{+27}_{-32}$	$192 \rightarrow 361$
	$\frac{\Delta m_{21}^2}{10^{-5} \text{ eV}^2}$	$7.42^{+0.21}_{-0.20}$	$6.82 \rightarrow 8.04$	$7.42^{+0.21}_{-0.20}$	$6.82 \rightarrow 8.04$
	$\frac{\Delta m_{3\ell}^2}{10^{-3} \text{ eV}^2}$	$+2.515^{+0.028}_{-0.028}$	$+2.431 \rightarrow +2.599$	$-2.498^{+0.028}_{-0.029}$	$-2.584 \rightarrow -2.413$
with SK atmospheric data					
	$\sin^2 \theta_{12}$	$0.304^{+0.012}_{-0.012}$	$0.269 \rightarrow 0.343$	$0.304^{+0.013}_{-0.012}$	$0.269 \rightarrow 0.343$
	$\theta_{12}/^\circ$	$33.45^{+0.77}_{-0.75}$	$31.27 \rightarrow 35.87$	$33.45^{+0.78}_{-0.75}$	$31.27 \rightarrow 35.87$
	$\sin^2 \theta_{23}$	$0.450^{+0.019}_{-0.016}$	$0.408 \rightarrow 0.603$	$0.570^{+0.016}_{-0.022}$	$0.410 \rightarrow 0.613$
	$\theta_{23}/^\circ$	$42.1^{+1.1}_{-0.9}$	$39.7 \rightarrow 50.9$	$49.0^{+0.9}_{-1.3}$	$39.8 \rightarrow 51.6$
	$\sin^2 \theta_{13}$	$0.02246^{+0.00062}_{-0.00062}$	$0.02060 \rightarrow 0.02435$	$0.02241^{+0.00074}_{-0.00062}$	$0.02055 \rightarrow 0.02457$
	$\theta_{13}/^\circ$	$8.62^{+0.12}_{-0.12}$	$8.25 \rightarrow 8.98$	$8.61^{+0.14}_{-0.12}$	$8.24 \rightarrow 9.02$
	$\delta_{\text{CP}}/^\circ$	$230^{+36}_{-25}$	$144 \rightarrow 350$	$278^{+22}_{-30}$	$194 \rightarrow 345$
	$\frac{\Delta m_{21}^2}{10^{-5} \text{ eV}^2}$	$7.42^{+0.21}_{-0.20}$	$6.82 \rightarrow 8.04$	$7.42^{+0.21}_{-0.20}$	$6.82 \rightarrow 8.04$
	$\frac{\Delta m_{3\ell}^2}{10^{-3} \text{ eV}^2}$	$+2.510^{+0.027}_{-0.027}$	$+2.430 \rightarrow +2.593$	$-2.490^{+0.026}_{-0.028}$	$-2.574 \rightarrow -2.410$

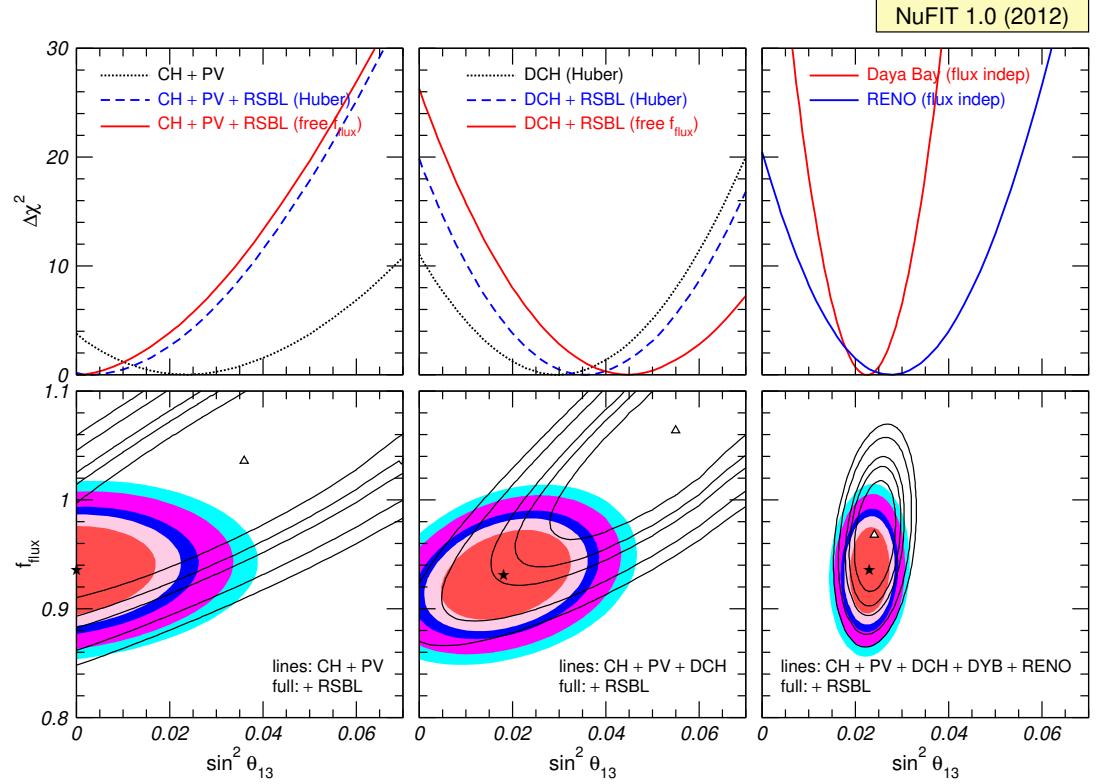


**Figure 2.** Dependence on the reactor flux normalization choice in NuFIT 1.0. **Upper:** Dependence of  $\Delta\chi^2$  on  $\sin^2 \theta_{13}$  (for fix value  $\Delta m_{31}^2 = 2.47 \times 10^{-3} \text{ eV}^2$ ) for the set of reactor experiments included in the analysis and three different assumptions on the fluxes as labeled in the figure. **Lower:** Confidence level contours in the plane of  $\sin^2 \theta_{13}$  and the flux normalization  $f_{\text{flux}}$ . Full regions and lines correspond to analysis with and without including the RSBL experiments respectively. Figure adapted from Ref. [31].

Being equipped with a near detector, the determination of  $\theta_{13}$  from Daya Bay and RENO was unaffected by the reactor anomaly. As their statistics increased, and with the entrance in operation of the Double Chooz near detector, the impact of the reactor flux normalization uncertainty steadily decreased, being reduced to  $\sim 0.5\sigma$  in the NuFIT 2.0 analysis and becoming essentially irrelevant in NuFIT 3.0.

In what respects the analysis of KamLAND long baseline reactor data, since NuFIT 4.0 we have been relying on the precise reconstruction of the reactor neutrino fluxes (both overall normalization and energy spectrum) provided by the Daya Bay near detectors [58], which renders also the KamLAND analysis largely independent of the reactor anomaly. As a side effect, this change in the KamLAND reactor flux model is responsible for the slight increase (from 14% to 16%) of the  $\Delta m_{21}^2$  uncertainty which can be observed in Eq. (5).

### 3.2. Status of $\Delta m_{21}^2$ in solar experiments versus KamLAND

The analyses of the solar experiments and of KamLAND give the dominant contribution to the determination of  $\Delta m_{21}^2$  and  $\theta_{12}$ . Starting with NuFIT 2.0, and as illustrated in the upper panels in Fig. 3, the results of the global analyses showed a value of  $\Delta m_{21}^2$  preferred by KamLAND which was somewhat higher than the value favoured by solar neutrino experiments. This tension arose from a combination of two effects which did not changed significantly till 2020:



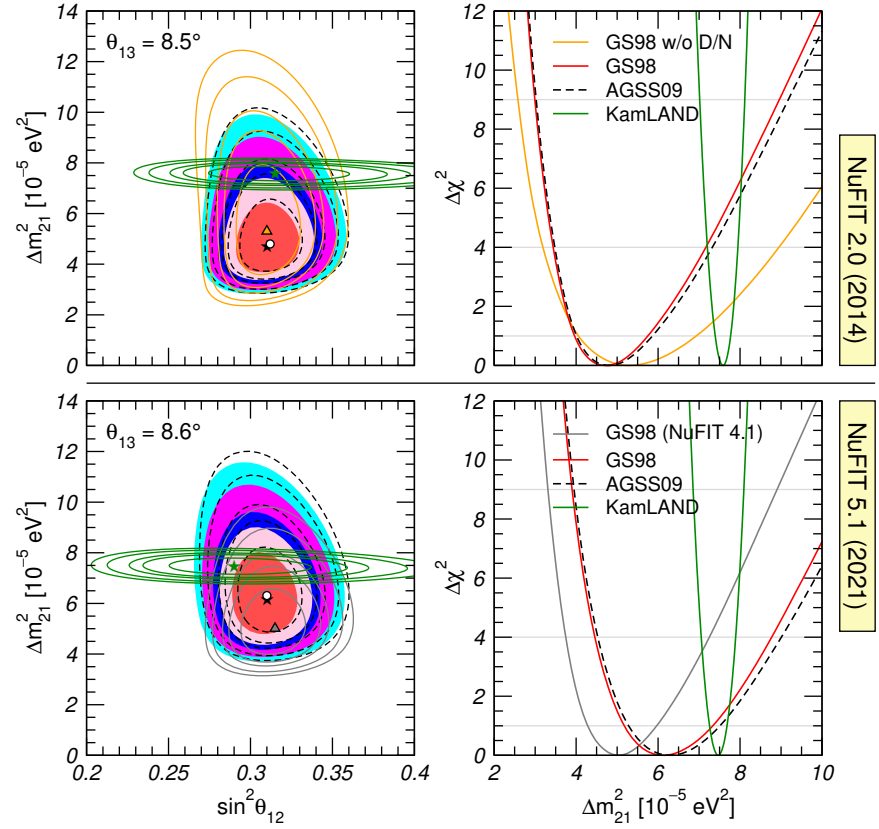


**Figure 3.** **Upper-left:** NuFIT 2.0 allowed parameter regions (at  $1\sigma$ , 90%,  $2\sigma$ , 99% and  $3\sigma$  CL for 2 d.o.f.) from the combined analysis of solar data for the GS98 model (full regions with best fit marked by black star) and the AGSS09 model (dashed void contours with best fit marked by a white dot), as well as for the analysis of KamLAND data (solid green contours with best fit marked by a green star) for fixed  $\theta_{13} = 8.5^\circ$ . We also show as orange contours the results of a global analysis for the GS98 model but without including the day-night information from SK. **Upper-right:** NuFIT 2.0  $\Delta\chi^2$  dependence on  $\Delta m_{21}^2$  for the same four analysis after marginalizing over  $\theta_{12}$ . **Lower-left:** Same as upper-left but for NuFIT 5.1 and fixed  $\theta_{13} = 8.6^\circ$ . Also show as orange contours the previous results of the global analysis for the GS98 model in NuFIT 4.0 [35]. **Lower-right:**  $\Delta\chi^2$  dependence on  $\Delta m_{21}^2$  for the same four analyses as the lower-left panel after marginalizing over  $\theta_{12}$ . Figure adapted from Ref. [30,32].

- the fact that the observed  $^8\text{B}$  spectrum at SNO, SK and Borexino showed no clear evidence of the low energy turn-up which is predicted to occur in the standard LMA-MSW [38,39] solution for the value of  $\Delta m_{21}^2$  which best fitted KamLAND;
- Super-Kamiokande observed a day-night asymmetry which was larger than expected for the  $\Delta m_{21}^2$  value preferred by KamLAND for which Earth matter effects are very small.

These effects resulted in the best fit value of  $\Delta m_{21}^2$  of KamLAND in the NuFIT 2.0 fit laying at the boundary of the  $2\sigma$  allowed range of the solar neutrino analysis as seen in the upper panels in Fig. 3. The tension was maintained with the increased statistics from SK-IV included in NuFIT 3.0 and the change of the reactor flux normalization used in the KamLAND analysis since NuFIT 4.0.

The tension was resolved with the latest SK4 2970-day results included in NuFIT 5.0 which were presented at the Neutrino2020 conference [13] in the form of their total energy

spectrum, which show a slightly more pronounced turn-up in the low energy part, and the updated day-night asymmetry

$$A_{D/N}^{\text{SK4-2970}} = (-2.1 \pm 1.1)\%. \quad (6)$$

which was lower than the previous reported value  $A_{D/N, \text{SK4-2055}} = [-3.1 \pm 1.6(\text{stat.}) \pm 1.4(\text{syst.})]\%$ .

The impact of these new data is displayed in the lower panels of Fig. 3. As can be seen, the tension between the best fit  $\Delta m_{21}^2$  of KamLAND and that of the solar results decreased and the preferred  $\Delta m_{21}^2$  value from KamLAND lies at  $\Delta\chi_{\text{solar}}^2 = 1.3$  (corresponding to  $1.1\sigma$ ). This decrease in the tension was due to both the smaller day-night asymmetry (which lowered  $\Delta\chi_{\text{solar}}^2$  of the KamLAND best fit  $\Delta m_{21}^2$  by 2.4 units) and the slightly more pronounced turn-up in the low energy part of the spectrum (which lowered it by one extra unit).

Finally, in order to quantify the independence of these results on the details of the solar modeling, the solar neutrino analysis in NuFIT were performed for the two versions of the Standard Solar Model, namely the GS98 and the AGSS09 models which result from employing two different determinations of the solar abundances [59,60]. As seen from the figure the determination of  $\Delta m_{21}^2$  and  $\theta_{12}$  is extremely robust over these variations on the modeling of the Sun.

### 3.3. Inclusion of Super-Kamiokande Atmospheric Neutrino Data

Atmospheric neutrinos are produced by the interaction of cosmic rays on the top of the Earth's atmosphere. In the subsequent hadronic cascades both  $\nu_e$  and  $\nu_\mu$  as well as  $\bar{\nu}_e$  and  $\bar{\nu}_\mu$  are produced. Furthermore, the neutrinos are produced in all possible directions and therefore at any detector positioned on the Earth a good fraction of the events generated by the interaction of these neutrinos correspond to neutrinos which have traveled through the Earth matter. For all these reasons atmospheric neutrinos constitute a powerful tool to study the evolution of neutrino flavour in their propagation.

In the context of three flavour oscillations, the atmospheric neutrino data show that the dominant oscillation channel of atmospheric neutrinos is  $\nu_\mu \rightarrow \nu_\tau$ , which in the standard convention described in Sec. 2 is driven by  $|\Delta m_{31}^2|$  and with the amplitude controlled by  $\theta_{23}$ . In principle, the flavour and neutrino and antineutrino composition of the atmospheric neutrino fluxes, together with the wide range of covered baselines, opens up the possibility of sensitivity to subleading oscillation modes, driven by  $\Delta m_{21}^2$  and/or  $\theta_{13}$ , especially in the light of the no-too-small value of  $\theta_{13}$ . In particular, they can potentially provide relevant information on the octant of  $\theta_{23}$ , on the value of  $\delta_{\text{CP}}$  and the ordering of the neutrino mass spectrum.

In NuFIT 1.0 and NuFIT 2.0 we performed our own analysis of the Super-Kamiokande atmospheric neutrino data for phases SK1–4. The analysis was based on the “classic” data samples — sub-GeV and multi-GeV  $e$ -like and  $\mu$ -like events, as well as partially-contained, stopping and through-going muons — which accounted for a total of 70 data points, and for which one could perform a reasonably accurate simulation using the information provided by the collaboration. The implications of our last SK analysis of such kind in the global picture is shown in Fig. 4: as can be seen, the impact on both the ordering and the determination of  $\Delta\chi^2$  was modest.

Around that time Super-Kamiokande started developing a dedicated analysis methodology aiming at constructing  $\nu_e + \bar{\nu}_e$  enriched atmospheric neutrino samples and to further classified them into  $\nu_e$ -like and  $\bar{\nu}_e$ -like subsamples. With those they seemed to succeed in increasing their sensitivity to the subleading effects. Unfortunately, with the limited information available outside of the collaboration it was not possible to reproduce the key elements driving the main dependence on these subdominant oscillation effects. Consequently our

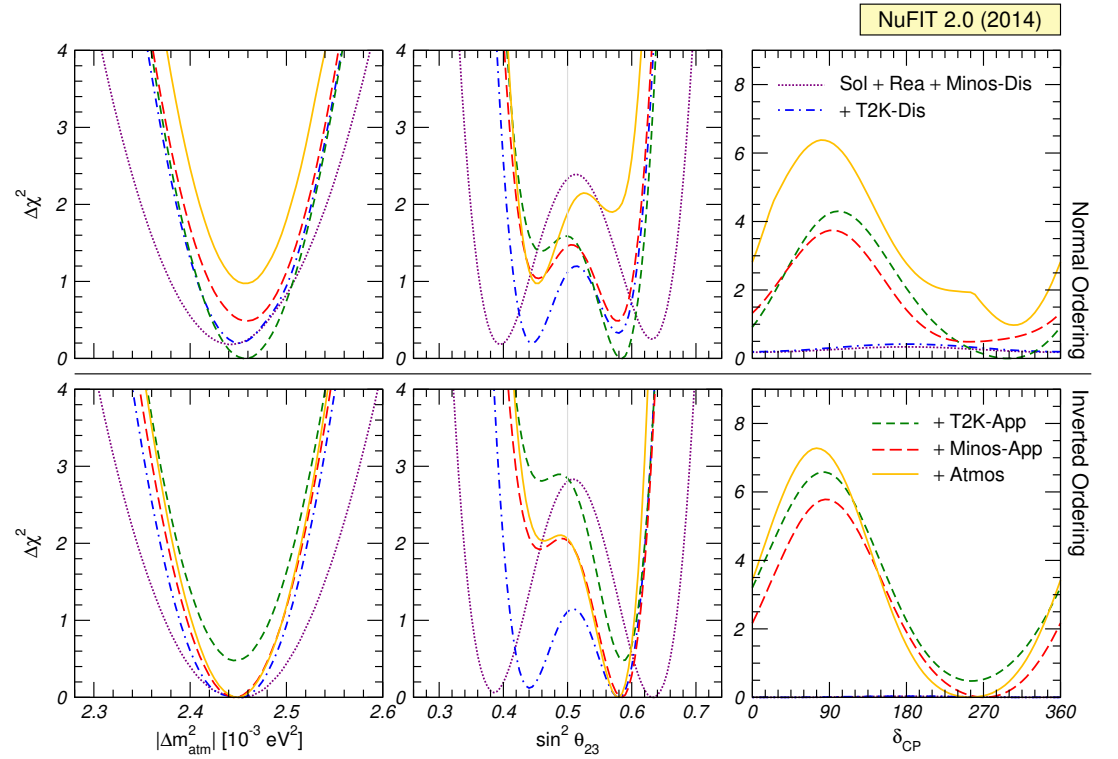


**Figure 4.** Contribution of different sets of experimental data included in NuFIT 2.0 to the determination of the mass ordering, the octant of  $\theta_{23}$  and the CP violating phase. Left (right) panels are for IO (NO). In the figure “Atmos” refers to our analysis of SK1–4 (including SK4 1775-day) combined data. Figure adapted from Ref. [32].

own simulation of the SK atmospheric data fell short at this task and since NuFIT-3.0 they were removed from our global analysis.

In 2017 the Super-Kamiokande collaboration started to publish results obtained with this method [4], providing also the corresponding tabulated  $\chi^2$  map [61] as a function of the four relevant parameters  $\Delta m^2_{3\ell}$ ,  $\theta_{23}$ ,  $\theta_{13}$ , and  $\delta_{CP}$ . Such table could be added to the  $\chi^2$  of our global analysis to address the impact of their data in the global picture. This was done in NuFIT 4.X and NuFIT 5.0 versions. Recently Super-Kamiokande has made public an updated table with a slight increase on the exposure [62]. The effect of adding that information has been included in our last analysis NuFIT 5.1 and it is shown as dashed curves in the right panels of Fig. 1. As seen in the figure (see also Table 2), the addition of SK-atm table to the latest analysis results into a increase of the favouring of NO and in the significance of CP violation, and a change in the favoured octant of  $\theta_{23}$ .

However, it should be noted that this procedure of “blindly adding” the  $\chi^2$  table as provided by the experimental collaboration is not optimal as it defeats the purpose of the global phenomenological analysis, whose aim is both reproducing and combining different data samples under a consistent set of assumptions on the theoretical uncertainties, as well as exploring the implication of the results in extended scenarios.

### 3.4. $\theta_{23}$ , $\delta_{CP}$ and mass ordering from LBL accelerator and MBL reactor experiments

From the point of view of the data included in the analysis, the most important variation over the last decade was in LBL accelerator and MBL reactor experiments.

The data included in NuFIT 1.0 for LBL experiments comprised the spectrum of  $\nu_\mu$  disappearance events of K2K [63], both  $\nu_\mu$  ( $\bar{\nu}_\mu$ ) disappearance and  $\nu_e$  ( $\bar{\nu}_e$ ) appearance spectra in MINOS with  $10.8 (3.36) \times 10^{20}$  protons on target (pot) [64], and the results from T2K  $\nu_e$  appearance and  $\nu_\mu$  disappearance data of phases 1-3 ( $3.01 \times 10^{20}$  pot [65]) and phases 1-2 ( $1.43 \times 10^{20}$  pot [66,67]), respectively. NOvA data was first available in NuFIT 3.0. NuFIT 5.X includes the latest results from T2K corresponding to  $19.7 \times 10^{20}$  pot ( $16.3 \times 10^{20}$  pot)  $\nu$  ( $\bar{\nu}$ ) spectra in both  $\nu_\mu$  ( $\bar{\nu}_\mu$ ) disappearance and  $\nu_e$  ( $\bar{\nu}_e$ ) appearance data [19], as well as NOvA's data corresponding to  $13.6 \times 10^{20}$  pot ( $12.5 \times 10^{20}$  pot)  $\nu$  ( $\bar{\nu}$ ) spectra in both  $\nu_\mu$  ( $\bar{\nu}_\mu$ ) disappearance and  $\nu_e$  ( $\bar{\nu}_e$ ) appearance [20]. In what respects the MBL reactor data, NuFIT 1.0 included the results of 126 live days of Daya Bay [68] and 229 days of data-taking of RENO [41] in the form of total event rates in the near and far detectors, together with the initial spectrum from Double Chooz far detector with 227.9 days live time [69,70]. In NuFIT 5.X we account for the results of the 1958-day EH2/EH1 and EH3/EH1 spectral ratios from Daya Bay [23], the 2908-day FD/ND spectral ratio from RENO [24], and the Double Chooz FD/ND spectral ratio with 1276-day (FD) and 587-day (ND) exposures [22].

The increase in the data available in both type of experiments, together with their complementarity, has been playing the leading role in the observation of subdominant effects associated to  $\delta_{\text{CP}}$ , to the neutrino mass ordering, and to the octant of  $\theta_{23}$ , with “hints” of favoured values and their statistical significance changing in time. We illustrate this in Fig. 5 where we show the  $\Delta\chi^2$  profiles as a function of these three parameters in the last two NuFIT analyses.

Qualitatively the most relevant effects can be understood in terms of approximate expressions for the relevant oscillation probabilities. In particular the  $\nu_\mu$  survival probability is given to good accuracy by [71,72]

$$P_{\mu\mu} \approx 1 - \sin^2 2\theta_{\mu\mu} \sin^2 \frac{\Delta m_{\mu\mu}^2 L}{4E_\nu}, \quad (7)$$

where  $L$  is the baseline,  $E_\nu$  is the neutrino energy, and

$$\sin^2 \theta_{\mu\mu} = \cos^2 \theta_{13} \sin^2 \theta_{23}, \quad (8)$$

$$\Delta m_{\mu\mu}^2 = \sin^2 \theta_{12} \Delta m_{31}^2 + \cos^2 \theta_{12} \Delta m_{32}^2 + \cos \delta_{\text{CP}} \sin \theta_{13} \sin 2\theta_{12} \tan \theta_{23} \Delta m_{21}^2. \quad (9)$$

Conversely the  $\nu_e$  survival probability relevant for reactor experiments with MBL can be approximated as [72,73]:

$$P_{ee} \approx 1 - \sin^2 2\theta_{13} \sin^2 \frac{\Delta m_{ee}^2 L}{4E_\nu}, \quad (10)$$

where

$$\Delta m_{ee}^2 = \cos^2 \theta_{12} \Delta m_{31}^2 + \sin^2 \theta_{12} \Delta m_{32}^2. \quad (11)$$

Hence, the determination of the oscillation frequencies in  $\nu_\mu$  and  $\nu_e$  disappearance experiments provides two independent measurements of the parameter  $|\Delta m_{3\ell}^2|$ , which already in NuFIT 2.0 were of similar accuracy and therefore allowed for a consistency test of the  $3\nu$  scenario. Furthermore, as precision increased the comparison of both oscillation frequencies started offering relevant information on the sign of  $\Delta m_{3\ell}^2$ , *i.e.*, contributing to the present sensitivity to the mass ordering.

For the  $\nu_e$  appearance results in T2K and NOvA, following Refs. [35,74], qualitative understanding can be obtained by expanding the appearance oscillation probability in the

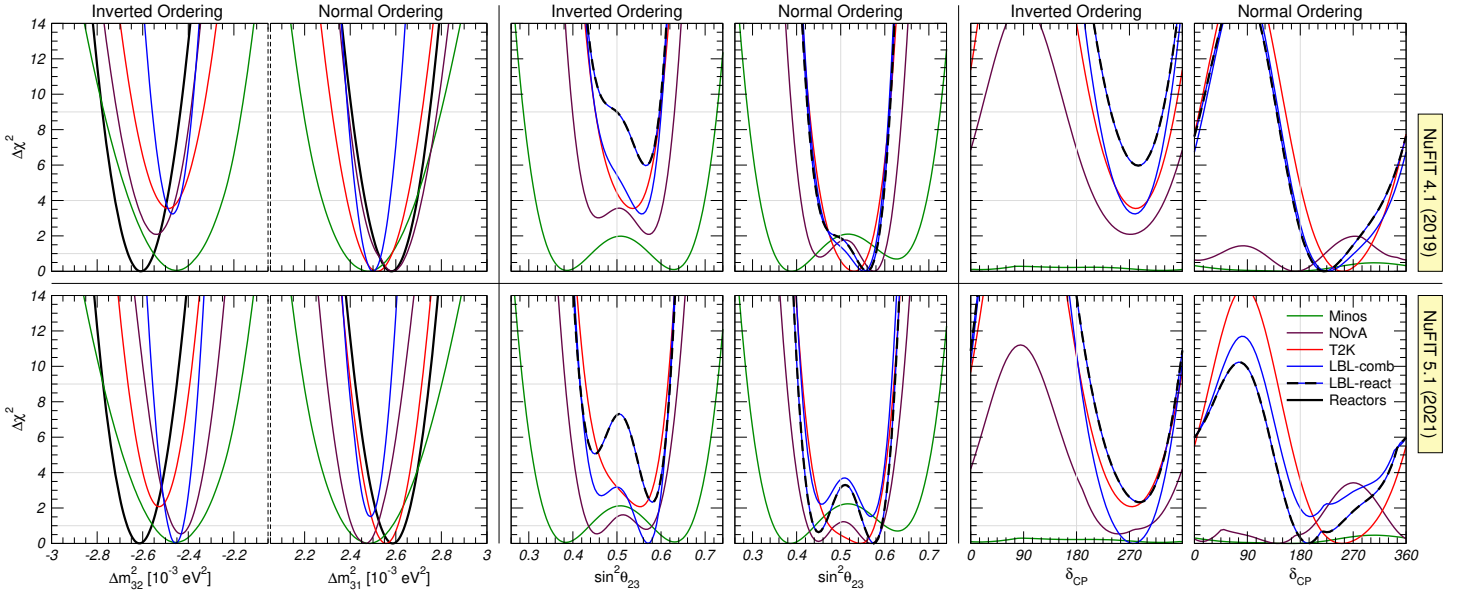


**Figure 5.**  $\Delta\chi^2$  profiles as a function of  $\Delta m_{3\ell}^2$  (left),  $\sin^2 \theta_{23}$  (center) and  $\delta_{CP}$  (right) for different LBL and reactor data sets and their combination obtained in NuFIT 4.1 and NuFIT 5.1. For all curves we have fixed  $\sin^2 \theta_{13} = 0.0224$  as well as the solar parameters and minimized with respect to the other undisplayed parameters.  $\Delta\chi^2$  is shown with respect to the best fit mass ordering for each curve. Figure adapted from Ref. [30,36].

small parameters  $\sin \theta_{13}$ ,  $\Delta m_{21}^2 L / E_\nu$ , and the matter potential term  $A \equiv |2E_\nu V / \Delta m_{3\ell}^2|$  ( $L$  is the baseline,  $E_\nu$  the neutrino energy and  $V$  the effective matter potential):

$$P_{\nu_\mu \rightarrow \nu_e} \approx 4s_{13}^2 s_{23}^2 (1 + 2sA) - C \sin \delta_{CP} (1 + sA), \quad (12)$$

$$P_{\bar{\nu}_\mu \rightarrow \bar{\nu}_e} \approx 4s_{13}^2 s_{23}^2 (1 - 2sA) + C \sin \delta_{CP} (1 - sA). \quad (13)$$

with  $s_{ij} \equiv \sin \theta_{ij}$  and

$$C \equiv \frac{\Delta m_{21}^2 L}{4E_\nu} \sin 2\theta_{12} \sin 2\theta_{13} \sin 2\theta_{23}, \quad s \equiv \text{sign}(\Delta m_{3\ell}^2), \quad (14)$$

and we have used  $|\Delta m_{3\ell}^2| L / 4E_\nu \approx \pi/2$  for both T2K and NOvA. Using the average value of the Earth crust matter density one finds that for neutrinos with mean energy at T2K  $A \approx 0.05$ , whereas for NOvA the approximation works best with an *empirical* value of  $A = 0.1$ . Under the approximation that the total number of appearance events observed in T2K and NOvA is proportional to the oscillation probability one can write

$$N_{\nu_e} \approx \mathcal{N}_\nu \left[ 2s_{23}^2 (1 + 2sA) - C' \sin \delta_{CP} (1 + sA) \right], \quad (15)$$

$$N_{\bar{\nu}_e} \approx \mathcal{N}_{\bar{\nu}} \left[ 2s_{23}^2 (1 - 2sA) + C' \sin \delta_{CP} (1 - sA) \right]. \quad (16)$$

When all the well-determined parameters  $\theta_{13}$ ,  $\theta_{12}$ ,  $\Delta m_{21}^2$ ,  $|\Delta m_{3\ell}^2|$  are set to their global best fit values, one gets  $C' \approx 0.28$  almost independently of the value of  $\theta_{23}$ . The normalization constants  $\mathcal{N}_{\nu, \bar{\nu}}$  can be calculated from the total number of events in the different appearance samples.

For the last few years, T2K data has been favouring a ratio of observed/expected events larger than 1 for neutrinos and smaller than 1 for anti-neutrinos. From the expressions in

Eq. (15) and (16) this implies that the square-bracket term in Eq. (15) had to be enhanced and the one in Eq. (16) had to be suppressed. With  $\theta_{13}$  fixed by reactor experiments, this could be achieved by choosing NO and  $\delta_{CP} \simeq 3\pi/2$ . This has been the driving factor for the hints in favour of NO and maximal CP violation since NuFIT 3.0. On the contrary, NOvA neutrino data has been pointing out towards ratios closer to 1 which can be accommodated by either (NO,  $\delta_{CP} \simeq \pi/2$ ) or (IO,  $\delta_{CP} \simeq 3\pi/2$ ). This behavior is consistent with NOvA anti-neutrinos, but the NO option is somewhat in tension with T2K. This small tension between T2K and NOvA has resulted into variations in the favoured ordering in the combined LBL analysis as well as the favoured octant of  $\theta_{23}$  and value of  $\delta_{CP}$  in NuFIT 4.X and NuFIT 5.X.

On the other hand, in what respects the accelerator/reactor complementary determination of the oscillation frequencies in  $\nu_\mu$  and  $\nu_e$  disappearance experiments, so far they have been consistently pointing towards a better agreement for NO than for IO, albeit within the limited statistical significance of the effect.

#### 4. Conclusions

Over the last two decades neutrino oscillation experiments have provided us with undoubted evidence that neutrinos have mass and that the lepton flavours mix in the charge current weak interaction of those massive states. Those observations, which cannot be explained within the Standard Model, represent our only laboratory evidence of physics beyond the Standard Model.

The determination of the flavour structure of the lepton sector at low energies is, at this point, our only source of information to understand the underlying BSM dynamics responsible for these observations, and it is therefore fundamental to ultimately establish the *New Standard Model*.

At present the task is at hands of phenomenological groups. NuFIT was formed in this context about 10 years ago as a fluid collaboration and since then it has provided updated results from the global analysis of neutrino oscillation measurements. The NuFIT analysis are performed in the framework of the Standard Model extended with three massive neutrinos, which is, at the moment, the minimal scenario capable of accommodating all oscillation result which have been robustly established. In this contribution we have summarized some results obtained by NuFIT over these decade, in particular describing those issues which were solved by new data and those which are still pending.

**Funding:** This work is supported by Spanish grants PID2019-105614GB-C21 and PID2019-110058GB-C21 financed by MCIN/AEI/10.13039/501100011033, by USA-NSF grant PHY-1915093, and by AGAUR (Generalitat de Catalunya) grant 2017-SGR-929. The authors acknowledge the support of European ITN grant H2020-MSCA-ITN-2019//860881-HIDDeN and of the Spanish Agencia Estatal de Investigación through the grant “IFT Centro de Excelencia Severo Ochoa SEV-2016-0597”.

#### References

1. Pontecorvo, B. Neutrino experiments and the question of leptonic-charge conservation. *Sov. Phys. JETP* **1968**, *26*, 984–988.
2. Gribov, V.N.; Pontecorvo, B. Neutrino astronomy and lepton charge. *Phys. Lett.* **1969**, *B28*, 493. doi:10.1016/0370-2693(69)90525-5.
3. Gonzalez-Garcia, M.C.; Maltoni, M. Phenomenology with Massive Neutrinos. *Phys. Rept.* **2008**, *460*, 1–129, [arXiv:hep-ph/0704.1800]. doi:10.1016/j.physrep.2007.12.004.
4. Abe, K.; others. Atmospheric Neutrino Oscillation Analysis with External Constraints in Super-Kamiokande I-IV. *Phys. Rev.* **2018**, *D97*, 072001, [arXiv:hep-ex/1710.09126]. doi:10.1103/PhysRevD.97.072001.
5. Aartsen, M.; others. Determining neutrino oscillation parameters from atmospheric muon neutrino disappearance with three years of IceCube DeepCore data. *Phys. Rev.* **2015**, *D91*, 072004, [arXiv:hep-ex/1410.7227]. doi:10.1103/PhysRevD.91.072004.
6. Yanez, J.P.; others. IceCube Oscillations: 3 years muon neutrino disappearance data. [http://icecube.wisc.edu/science/data/nu\\_osc](http://icecube.wisc.edu/science/data/nu_osc).
7. Cleveland, B.T.; others. Measurement of the solar electron neutrino flux with the Homestake chlorine detector. *Astrophys. J.* **1998**, *496*, 505–526. doi:10.1086/305343.



8. Kaether, F.; Hampel, W.; Heusser, G.; Kiko, J.; Kirsten, T. Reanalysis of the GALLEX solar neutrino flux and source experiments. *Phys. Lett.* **2010**, *B685*, 47–54, [arXiv:hep-ex/1001.2731]. doi:10.1016/j.physletb.2010.01.030.
9. Abdurashitov, J.N.; others. Measurement of the solar neutrino capture rate with gallium metal. III: Results for the 2002–2007 data-taking period. *Phys. Rev.* **2009**, *C80*, 015807, [arXiv:nucl-ex/0901.2200]. doi:10.1103/PhysRevC.80.015807.
10. Hosaka, J.; others. Solar neutrino measurements in Super-Kamiokande-I. *Phys. Rev.* **2006**, *D73*, 112001, [hep-ex/0508053]. doi:10.1103/PhysRevD.73.112001.
11. Cravens, J.; others. Solar neutrino measurements in Super-Kamiokande-II. *Phys. Rev.* **2008**, *D78*, 032002, [arXiv:hep-ex/0803.4312]. doi:10.1103/PhysRevD.78.032002.
12. Abe, K.; others. Solar neutrino results in Super-Kamiokande-III. *Phys. Rev.* **2011**, *D83*, 052010, [arXiv:hep-ex/1010.0118]. doi:10.1103/PhysRevD.83.052010.
13. Nakajima, Y. SuperKamiokande. Talk given at the XXIX International Conference on Neutrino Physics and Astrophysics, Chicago, USA, June 22–July 2, 2020 (online conference) doi.org/10.5281/zenodo.3959640, doi:10.5281/zenodo.3959640.
14. Aharmim, B.; others. Combined Analysis of All Three Phases of Solar Neutrino Data from the Sudbury Neutrino Observatory. *Phys. Rev.* **2013**, *C88*, 025501, [arXiv:nucl-ex/1109.0763]. doi:10.1103/PhysRevC.88.025501.
15. Bellini, G.; others. Precision measurement of the  $^7\text{Be}$  solar neutrino interaction rate in Borexino. *Phys. Rev. Lett.* **2011**, *107*, 141302, [arXiv:hep-ex/1104.1816]. doi:10.1103/PhysRevLett.107.141302.
16. Bellini, G.; others. Measurement of the solar  $^8\text{B}$  neutrino rate with a liquid scintillator target and 3 MeV energy threshold in the Borexino detector. *Phys. Rev.* **2010**, *D82*, 033006, [arXiv:astro-ph/0808.2868]. doi:10.1103/PhysRevD.82.033006.
17. Bellini, G.; others. Neutrinos from the primary proton–proton fusion process in the Sun. *Nature* **2014**, *512*, 383–386. doi:10.1038/nature13702.
18. Adamson, P.; others. Measurement of Neutrino and Antineutrino Oscillations Using Beam and Atmospheric Data in MINOS. *Phys. Rev. Lett.* **2013**, *110*, 251801, [arXiv:hep-ex/1304.6335]. doi:10.1103/PhysRevLett.110.251801.
19. Dunne, P. Latest Neutrino Oscillation Results from T2K. Talk given at the XXIX International Conference on Neutrino Physics and Astrophysics, Chicago, USA, June 22–July 2, 2020 (online conference) doi.org/10.5281/zenodo.3959558, doi:10.5281/zenodo.3959558.
20. Himmel, A. New Oscillation Results from the NOvA Experiment. Talk given at the XXIX International Conference on Neutrino Physics and Astrophysics, Chicago, USA, June 22–July 2, 2020 (online conference) doi.org/10.5281/zenodo.3959581, doi:10.5281/zenodo.3959581.
21. Adamson, P.; others. Electron neutrino and antineutrino appearance in the full MINOS data sample. *Phys. Rev. Lett.* **2013**, [arXiv:hep-ex/1301.4581]. doi:10.1103/PhysRevLett.110.171801.
22. Bezerra, T. New Results from the Double Chooz Experiment. Talk given at the XXIX International Conference on Neutrino Physics and Astrophysics, Chicago, USA, June 22–July 2, 2020 (online conference) doi.org/10.5281/zenodo.3959542, doi:10.5281/zenodo.3959542.
23. Adey, D.; others. Measurement of Electron Antineutrino Oscillation with 1958 Days of Operation at Daya Bay. *Phys. Rev. Lett.* **2018**, *121*, 241805, [arXiv:hep-ex/1809.02261]. doi:10.1103/PhysRevLett.121.241805.
24. Yoo, J. RENO. Talk given at the XXIX International Conference on Neutrino Physics and Astrophysics, Chicago, USA, June 22–July 2, 2020 (online conference) doi.org/10.5281/zenodo.3959698, doi:10.5281/zenodo.3959698.
25. Gando, A.; others. Reactor On-Off Antineutrino Measurement with Kamland. *Phys. Rev.* **2013**, *D88*, 033001, [arXiv:hep-ex/1303.4667]. doi:10.1103/PhysRevD.88.033001.
26. de Salas, P.; Forero, D.; Gariazzo, S.; Martinez-Mirave, P.; Mena, O.; Ternes, C.; Tortola, M.; Valle, J. 2020 Global Reassessment of the Neutrino Oscillation Picture **2020**. [arXiv:hep-ph/2006.11237].
27. De Salas, P.; Gariazzo, S.; Mena, O.; Ternes, C.; Tortola, M. Neutrino Mass Ordering from Oscillations and Beyond: 2018 Status and Future Prospects. *Front. Astron. Space Sci.* **2018**, *5*, 36, [arXiv:hep-ph/1806.11051]. doi:10.3389/fspas.2018.00036.
28. Capozzi, F.; Di Valentino, E.; Lisi, E.; Marrone, A.; Melchiorri, A.; Palazzo, A. Addendum To: Global Constraints on Absolute Neutrino Masses and Their Ordering **2020**. [arXiv:hep-ph/2003.08511]. [Addendum: Phys.Rev.D 101, 116013 (2020)], doi:10.1103/PhysRevD.101.116013.
29. Capozzi, F.; Lisi, E.; Marrone, A.; Palazzo, A. Current Unknowns in the Three Neutrino Framework. *Prog. Part. Nucl. Phys.* **2018**, *102*, 48–72, [arXiv:hep-ph/1804.09678]. doi:10.1016/j.pnpnp.2018.05.005.
30. NuFit webpage. <http://www.nu-fit.org>.
31. Gonzalez-Garcia, M.; Maltoni, M.; Salvado, J.; Schwetz, T. Global fit to three neutrino mixing: critical look at present precision. *JHEP* **2012**, *1212*, 123, [arXiv:hep-ph/1209.3023]. doi:10.1007/JHEP12(2012)123.
32. Gonzalez-Garcia, M.C.; Maltoni, M.; Schwetz, T. Updated Fit to Three Neutrino Mixing: Status of Leptonic CP Violation. *JHEP* **2014**, *11*, 052, [arXiv:hep-ph/1409.5439]. doi:10.1007/JHEP11(2014)052.
33. Bergstrom, J.; Gonzalez-Garcia, M.C.; Maltoni, M.; Schwetz, T. Bayesian global analysis of neutrino oscillation data. *JHEP* **2015**, *09*, 200, [arXiv:hep-ph/1507.04366]. doi:10.1007/JHEP09(2015)200.
34. Esteban, I.; Gonzalez-Garcia, M.C.; Maltoni, M.; Martínez-Soler, I.; Schwetz, T. Updated Fit to Three Neutrino Mixing: Exploring the Accelerator-Reactor Complementarity. *JHEP* **2017**, *01*, 087, [arXiv:hep-ph/1611.01514]. doi:10.1007/JHEP01(2017)087.

35. Esteban, I.; Gonzalez-Garcia, M.C.; Hernandez-Cabezudo, A.; Maltoni, M.; Schwetz, T. Global analysis of three-flavour neutrino oscillations: synergies and tensions in the determination of  $\theta_{23}$ ,  $\delta_{CP}$ , and the mass ordering. *JHEP* **2019**, *01*, 106, [arXiv:hep-ph/1811.05487]. doi:10.1007/JHEP01(2019)106.
36. Esteban, I.; Gonzalez-Garcia, M.C.; Maltoni, M.; Schwetz, T.; Zhou, A. The fate of hints: updated global analysis of three-flavor neutrino oscillations. *JHEP* **2020**, *09*, 178, [arXiv:hep-ph/2007.14792]. doi:10.1007/JHEP09(2020)178.
37. Tanabashi, M.; others. Review of Particle Physics. *Phys. Rev. D* **2018**, *98*, 030001. doi:10.1103/PhysRevD.98.030001.
38. Wolfenstein, L. Neutrino oscillations in matter. *Phys. Rev.* **1978**, *D17*, 2369–2374. doi:10.1103/PhysRevD.17.2369.
39. Mikheev, S.P.; Smirnov, A.Y. Resonance enhancement of oscillations in matter and solar neutrino spectroscopy. *Sov. J. Nucl. Phys.* **1985**, *42*, 913–917.
40. An, F.; others. Observation of electron-antineutrino disappearance at Daya Bay. *Phys.Rev.Lett.* **2012**, *108*, 171803, [arXiv:hep-ex/1203.1669]. doi:10.1103/PhysRevLett.108.171803.
41. Ahn, J.; others. Observation of Reactor Electron Antineutrino Disappearance in the RENO Experiment. *Phys.Rev.Lett.* **2012**, *108*, 191802, [arXiv:hep-ex/1204.0626]. doi:10.1103/PhysRevLett.108.191802.
42. Abe, Y.; others. Indication for the disappearance of reactor electron antineutrinos in the Double Chooz experiment. *Phys.Rev.Lett.* **2012**, *108*, 131801, [arXiv:hep-ex/1112.6353]. doi:10.1103/PhysRevLett.108.131801.
43. Apollonio, M.; others. Limits on Neutrino Oscillations from the CHOOZ Experiment. *Phys. Lett.* **1999**, *B466*, 415–430, [hep-ex/9907037]. doi:10.1016/S0370-2693(99)01072-2.
44. Piepke, A. Final results from the Palo Verde neutrino oscillation experiment. *Prog. Part. Nucl. Phys.* **2002**, *48*, 113–121. doi:10.1016/S0146-6410(02)00117-5.
45. Mueller, T.; Lhuillier, D.; Fallot, M.; Letourneau, A.; Cormon, S.; others. Improved Predictions of Reactor Antineutrino Spectra. *Phys.Rev.* **2011**, *C83*, 054615, [arXiv:hep-ex/1101.2663]. doi:10.1103/PhysRevC.83.054615.
46. Huber, P. On the determination of anti-neutrino spectra from nuclear reactors. *Phys.Rev.* **2011**, *C84*, 024617, [arXiv:hep-ph/1106.0687]. doi:10.1103/PhysRevC.85.029901, 10.1103/PhysRevC.84.024617.
47. Mention, G.; Fechner, M.; Lasserre, T.; Mueller, T.; Lhuillier, D.; others. The Reactor Antineutrino Anomaly. *Phys.Rev.* **2011**, *D83*, 073006, [arXiv:hep-ex/1101.2755]. doi:10.1103/PhysRevD.83.073006.
48. Declais, Y.; de Kerret, H.; Lefievre, B.; Obolensky, M.; Etenko, A.; others. Study of reactor anti-neutrino interaction with proton at Bugey nuclear power plant. *Phys.Lett.* **1994**, *B338*, 383–389. doi:10.1016/0370-2693(94)91394-3.
49. Kuvshinnikov, A.; Mikaelyan, L.; Nikolaev, S.; Skorokhvatov, M.; Etenko, A. Measuring the  $\bar{\nu}_e + p \rightarrow n + e^+$  cross-section and beta decay axial constant in a new experiment at Rovno NPP reactor. (In Russian). *JETP Lett.* **1991**, *54*, 253–257.
50. Declais, Y.; Favier, J.; Metref, A.; Pessard, H.; Achkar, B.; others. Search for neutrino oscillations at 15-meters, 40-meters, and 95-meters from a nuclear power reactor at Bugey. *Nucl.Phys.* **1995**, *B434*, 503–534. doi:10.1016/0550-3213(94)00513-E.
51. Vidyakin, G.; Vyrodov, V.; Gurevich, I.; Kozlov, Y.; Martemyanov, V.; others. DETECTION OF ANTI-NEUTRINOS IN THE FLUX FROM TWO REACTORS. *Sov.Phys.JETP* **1987**, *66*, 243–247.
52. Vidyakin, G.; Vyrodov, V.; Kozlov, Y.; Martemyanov, A.; Martemyanov, V.; others. Limitations on the characteristics of neutrino oscillations. *JETP Lett.* **1994**, *59*, 390–393.
53. Kwon, H.; Boehm, F.; Hahn, A.; Henriksen, H.; Vuilleumier, J.; others. SEARCH FOR NEUTRINO OSCILLATIONS AT A FISSION REACTOR. *Phys.Rev.* **1981**, *D24*, 1097–1111. doi:10.1103/PhysRevD.24.1097.
54. Zacek, G.; others. Neutrino Oscillation Experiments at the Gosgen Nuclear Power Reactor. *Phys.Rev.* **1986**, *D34*, 2621–2636. doi:10.1103/PhysRevD.34.2621.
55. Greenwood, Z.D.; others. Results of a two position reactor neutrino oscillation experiment. *Phys. Rev.* **1996**, *D53*, 6054–6064. doi:10.1103/PhysRevD.53.6054.
56. Afonin, A.; Ketov, S.; Kopeikin, V.; Mikaelyan, L.; Skorokhvatov, M.; others. A study of the reaction  $\bar{\nu}_e + p \rightarrow e^+ + n$  on a nuclear reactor. *Sov.Phys.JETP* **1988**, *67*, 213–221.
57. Schwetz, T.; Tortola, M.; Valle, J. Global neutrino data and recent reactor fluxes: status of three-flavour oscillation parameters. *New J.Phys.* **2011**, *13*, 063004, [arXiv:hep-ph/1103.0734]. doi:10.1088/1367-2630/13/6/063004.
58. An, F.P.; others. Improved Measurement of the Reactor Antineutrino Flux and Spectrum at Daya Bay. *Chin. Phys.* **2017**, *C41*, 013002, [arXiv:hep-ex/1607.05378]. doi:10.1088/1674-1137/41/1/013002.
59. Vinyoles, N.; Serenelli, A.M.; Villante, F.L.; Basu, S.; Bergström, J.; Gonzalez-Garcia, M.C.; Maltoni, M.; Peña-Garay, C.; Song, N. A new Generation of Standard Solar Models. *Astrophys. J.* **2017**, *835*, 202, [arXiv:astro-ph.SR/1611.09867]. doi:10.3847/1538-4357/835/2/202.
60. Bergstrom, J.; Gonzalez-Garcia, M.C.; Maltoni, M.; Pena-Garay, C.; Serenelli, A.M.; Song, N. Updated determination of the solar neutrino fluxes from solar neutrino data. *JHEP* **2016**, *03*, 132, [arXiv:hep-ph/1601.00972]. doi:10.1007/JHEP03(2016)132.
61. Atmospheric neutrino oscillation analysis with external constraints in Super-Kamiokande I-IV. link to data release: <http://www-sk.icrr.u-tokyo.ac.jp/skdata/>
62. SK Atmospheric Oscillation Analysis 2020 (preliminary) results. link to data release: <https://indico-sk.icrr.u-tokyo.ac.jp/indico/event2020/>
63. Ahn, M.H.; others. Measurement of Neutrino Oscillation by the K2K Experiment. *Phys. Rev.* **2006**, *D74*, 072003, [hep-ex/0606032]. doi:10.1103/PhysRevD.74.072003.

- 
64. Nichols, R. Talk given at the XXV *International Conference on Neutrino Physics*, Kyoto, Japan, June 3–9, 2012.
  65. Sakashita, K. Talk given at the 36th *International Conference on High Energy Physics*, Melbourne, Australia, July 4–11, 2012.
  66. Abe, K.; others. First Muon-Neutrino Disappearance Study with an Off-Axis Beam. *Phys.Rev.* **2012**, *D85*, 031103, [[arXiv:hep-ex/1201.1386](#)]. doi:10.1103/PhysRevD.85.031103.
  67. Nakaya, T. Talk given at the XXV *International Conference on Neutrino Physics*, Kyoto, Japan, June 3–9, 2012.
  68. Dwyer, D. Improved measurement of electron-antineutrino disappearance at Daya Bay. Talk given at the XXV *International Conference on Neutrino Physics*, Kyoto, Japan, June 3–9, 2012.
  69. Abe, Y.; others. Reactor electron antineutrino disappearance in the Double Chooz experiment **2012**. [[arXiv:hep-ex/1207.6632](#)].
  70. Ishitsuka, M. Talk given at the XXV *International Conference on Neutrino Physics*, Kyoto, Japan, June 3–9, 2012.
  71. Okamura, N. Effect of the Smaller Mass-Squared Difference for the Long Base-Line Neutrino Experiments. *Prog. Theor. Phys.* **2006**, *114*, 1045–1056, [[arXiv:hep-ph/hep-ph/0411388](#)]. doi:10.1143/PTP.114.1045.
  72. Nunokawa, H.; Parke, S.J.; Zukanovich Funchal, R. Another Possible Way to Determine the Neutrino Mass Hierarchy. *Phys. Rev.* **2005**, *D72*, 013009, [[arXiv:hep-ph/hep-ph/0503283](#)]. doi:10.1103/PhysRevD.72.013009.
  73. Minakata, H.; Nunokawa, H.; Parke, S.J.; Zukanovich Funchal, R. Determining Neutrino Mass Hierarchy by Precision Measurements in Electron and Muon Neutrino Disappearance Experiments. *Phys. Rev.* **2006**, *D74*, 053008, [[arXiv:hep-ph/hep-ph/0607284](#)]. doi:10.1103/PhysRevD.74.053008.
  74. Elevant, J.; Schwetz, T. On the determination of the leptonic CP phase. *JHEP* **2015**, *09*, 016, [[arXiv:hep-ph/1506.07685](#)]. doi:10.1007/JHEP09(2015)016.